Article

Molecular Cell

A Precise Cdk Activity Threshold Determines Passage through the Restriction Point

Graphical Abstract

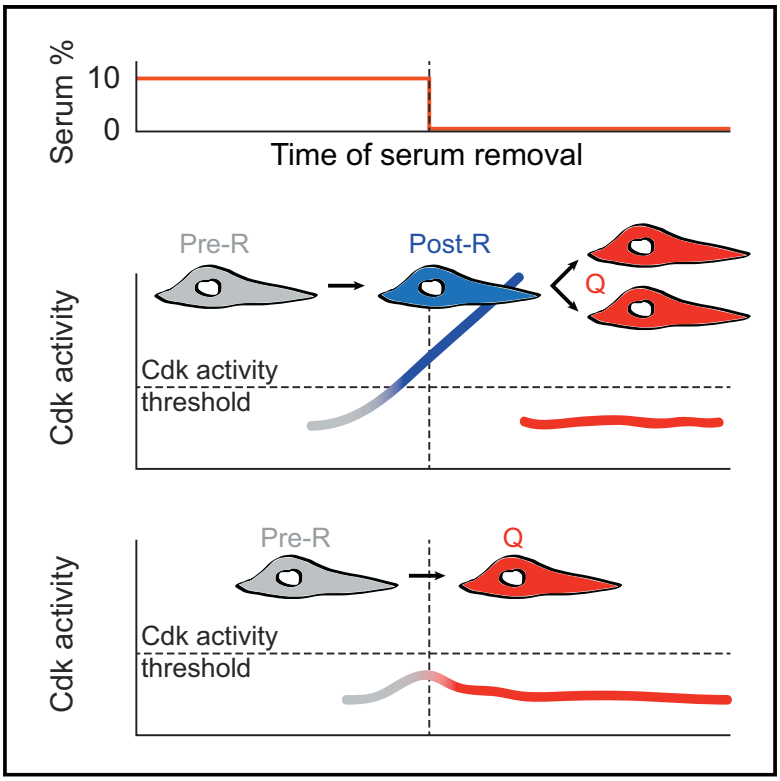

Authors

Clayton Schwarz, Amy Johnson, Mardo Kõivomägi, Evgeny Zatulovskiy, Carolyn J. Kravitz, Andreas Doncic, Jan M. Skotheim

Correspondence

skotheim@stanford.edu

In Brief

Schwarz et al. examine the responses of primary cells expressing a live-cell Cdk activity sensor to growth factor removal. They find that Cdk activity at the time of growth factor removal is an accurate predictor of whether a cell subsequently divides.

Highlights

- Primary fibroblast cell-cycle commitment with respect to serum removal (R) is in G1
- Cultured immortal cell lines mostly commit to division in the previous cell cycle
- R can be accurately predicted by measuring Cdk activity before serum removal
- HDHB fragment senses Cdk2 and Cdk1 in complex with either cyclin E or A

Schwarz et al., 2018, Molecular Cell 69, 253–264
January 18, 2018
https://doi.org/10.1016/j.molcel.2017.12.017

CellPress

Molecular Cell
Article

CellPress

A Precise Cdk Activity Threshold Determines Passage through the Restriction Point

Clayton Schwarz,[1] Amy Johnson,[1] Mardo Kõivomägi,[1] Evgeny Zatulovskiy,[1] Carolyn J. Kravitz,[1] Andreas Doncic,[2] and Jan M. Skotheim[1,3,*]
[1]Department of Biology, Stanford University, Stanford, CA 94305, USA
[2]Department of Cell Biology & Green Center for Systems Biology, UT Southwestern Medical Center, Dallas, TX 75390, USA
[3]Lead Contact
*Correspondence: skotheim@stanford.edu
https://doi.org/10.1016/j.molcel.2017.12.017

SUMMARY

At the restriction point (R), mammalian cells irreversibly commit to divide. R has been viewed as a point in G1 that is passed when growth factor signaling initiates a positive feedback loop of Cdk activity. However, recent studies have cast doubt on this model by claiming R occurs prior to positive feedback activation in G1 or even before completion of the previous cell cycle. Here we reconcile these results and show that whereas many commonly used cell lines do not exhibit a G1 R, primary fibroblasts have a G1 R that is defined by a precise Cdk activity threshold and the activation of cell-cycle-dependent transcription. A simple threshold model, based solely on Cdk activity, predicted with more than 95% accuracy whether individual cells had passed R. That a single measurement accurately predicted cell fate shows that the state of complex regulatory networks can be assessed using a few critical protein activities.

INTRODUCTION

In mammalian cells, growth factor signaling is required for cell-cycle progression up to the restriction point (R) (Pardee, 1974, 1989; Planas-Silva and Weinberg, 1997). Beyond R, cells will progress through to division even if growth factors are removed from the extracellular environment. R therefore marks the point of irreversible commitment to division. Due to its importance in the regulation of cell proliferation, mutations weakening or eliminating R characterize all forms of cancer (Pardee et al., 1978; Sherr, 2000; Zetterberg et al., 1995). Despite its importance to both normal development and disease, we currently lack a consensus as to when in the cell cycle R occurs and what constitutes its molecular basis.

R was originally determined to occur in late G1 just prior to the initiation of DNA replication (Pardee, 1974; Yen and Pardee, 1978). According to the current consensus, progression through G1 is initially driven by growth factor signaling that increases the expression of cyclin D (Planas-Silva and Weinberg, 1997; Sherr, 2000). Cyclin D-Cdk4/6 complexes mono-phosphorylate the transcriptional inhibitor Rb (Narasimha et al., 2014). While the function of this Rb mono-phosphorylation is presently unclear, cyclin D-Cdk4/6 likely promotes division through the partial inactivation of Rb. This frees E2F transcription factors, which then promote the expression of downstream cyclins E and A that activate Cdk2 to complete Rb inactivation and initiate E2F-dependent transcriptional activation. The E2F-Rb-cyclin E circuit is a positive feedback loop in which E2F and cyclin E activate their own expression and drive cells into S phase (Geng et al., 1996; Johnson et al., 1994; Spencer et al., 2013). In this positive feedback model for R, once threshold levels of active E2F and cyclin E are reached, they can stimulate and maintain their own expression so that cells become insensitive to decreases in upstream growth factor signaling (Yao et al., 2008). In support of this model, reducing positive feedback inhibitors, such as Rb, p27, or p21, decreases the amount of growth factor signaling required for proliferation (Coats et al., 1996; Hitomi et al., 2006; Polyak et al., 1994; Sage et al., 2000; Sherr and Roberts, 1999; Zwang et al., 2011), while reducing positive feedback activators, such as Cdk2 or cyclin D, has the opposite effect (Hitomi and Stacey, 1999; Lee et al., 2010; Merrick et al., 2011). Moreover, increasing feedback activators, such as cyclins D and E, can lead to immediate triggering of the positive feedback loop (Naetar et al., 2014; Quelle et al., 1993; Spencer et al., 2013).

While the E2F-Rb-cyclin E feedback loop presents an appealing mechanism for an irreversible transition driving a cell into S phase, recent single-cell analyses cast doubt on this model (Martinsson et al., 2005; Spencer et al., 2013). One study suggested that R takes place in G1 approximately 5 hr before Rb hyperphosphorylation, implying that R and positive feedback activation are two temporally distinct events (Martinsson et al., 2005). Another recent study found that many cells committed to division before completing mitosis in the previous cell cycle (Spencer et al., 2013). Thus, although much has been learned about molecular aspects of cell-cycle control, how and when cells commit to division remains controversial (Foster et al., 2010).

Here we aim to provide a unified, consistent model of R that can reconcile the disparate observations discussed above. We find evidence that in primary fibroblasts, R is located in G1 and is associated with the activation of the Rb-E2F-Cdk positive feedback loop.

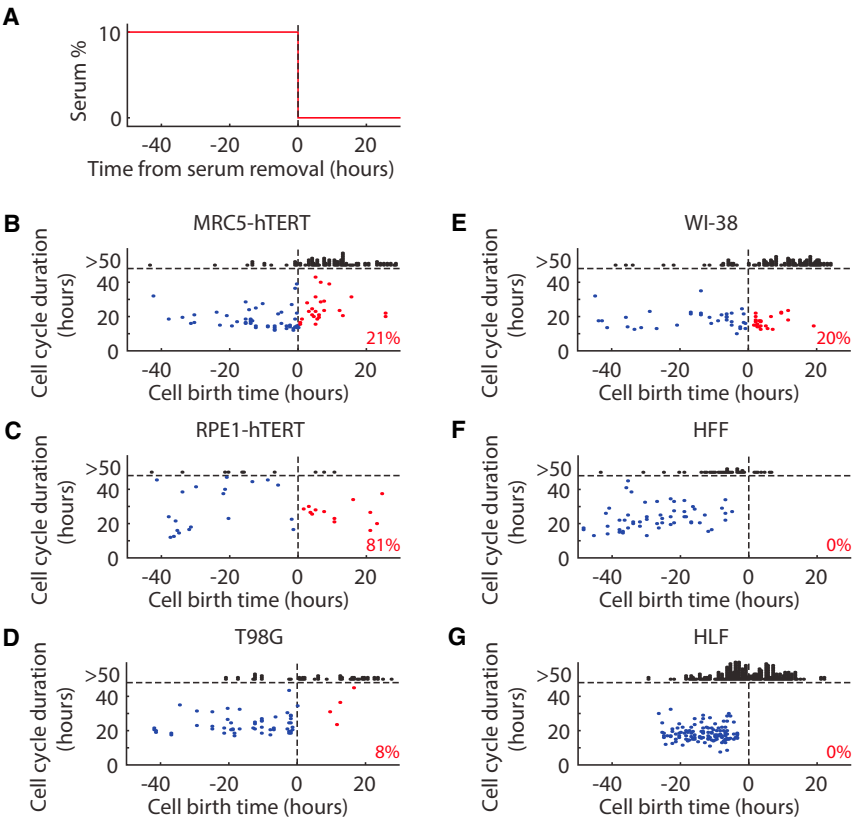

Figure 1. Primary Fibroblasts, but Not Cell Lines, Exhibit a Serum-Dependent G1 R

(A) Experiment schematic: cells were grown and imaged for 2 days in medium with 10% serum. Then, serum was removed.

(B–G) Birth times relative to the time of serum removal and cell-cycle durations were measured for (B) MRC5-hTERT cells (n = 206), (C) RPE1-hTERT cells (n = 43), (D) T98G cells (n = 124), (E) WI-38 cells (n = 171), (F) primary human foreskin fibroblasts (HFF; n = 93), and (G) primary human lung fibroblasts (HLF; n = 376). Horizontal dashed lines denote cell-cycle durations greater than 50 hr. Black dots indicate cells that did not divide again. Blue dots indicate cells born into serum-containing medium that went on to divide. Red dots indicate cells born into serum-free medium that went on to divide. The percentage of cells born into serum-free medium that went on to divide is indicated.

RESULTS

Primary Fibroblasts, but Not Cell Lines, Exhibit a Serum-Dependent G1 R

Motivated by the current disagreement over the timing and mechanism of R, we first sought to more accurately determine when R occurs in the cell cycle. Following Martinsson et al. (2005), we used live-cell time-lapse microscopy to track asynchronously dividing single cells as they respond to abrupt serum removal (Figure 1A). This method achieves higher temporal resolution than population-based methods and minimizes stressful perturbations associated with cell-cycle synchronization. Cells were first grown for 2 days in the presence of 10% serum, which provides growth factor stimulation. Then, cells were switched to serum-free medium and imaged for an additional 2 days. We classify cells that divide once more in serum-free medium as post-R and cells that arrest their cell cycle as pre-R. As a control we measured cell-cycle durations for cells where the medium was replaced with serum-containing medium. Cell-cycle durations were unaffected by medium exchange (Figures S1A–S1C).

Using this single-cell assay, we attempted to measure the timing of R in several frequently used cell lines. Surprisingly, some cells born after serum removal from each of these cell lines subsequently divided; i.e., none of these cell lines had a distinct serum-dependent R in G1 (Figures 1B–1E). We examined asynchronously cycling cells from lines derived from human fetal lung fibroblasts (WI-38 and MRC5-hTert), as well as a cell line derived from retinal epithelial cells (RPE1-hTert) and a glioblastoma line considered to have a fairly normal response to serum removal (T98G) (Stein, 1979). Many cells born after serum was removed went on to divide again, indicating that they do not need serum stimulation at any time during G1 to divide (red cells to the right of the dashed lines in Figures 1B–1E). This meant that many cells were already committed to divide at least twice before the end of the previous cell cycle. Similar single-cell results have been reported for three other cell lines (Spencer et al., 2013). This suggests that the process of cell line creation often selects for the ability to bypass R.

Unlike these cell lines, recently isolated primary human foreskin fibroblasts (HFFs) and human lung fibroblasts (HLFs) had a G1 R (Figures 1F and 1G). Both primary mouse embryonic fibroblasts (MEFs) and 3T3-immortalized MEFs are more similar to primary human fibroblasts than to the other cell lines in their response to serum removal (Figures S1D and S1E). All subsequent analyses were performed with HLFs.

The Timing of Primary Fibroblast Passage through R Is Variable

In order to determine the timing of passage through R, we measured the fraction of cells that went on to divide after serum removal as a function of cell age at the time of serum removal (Figure 2A). All cells less than 3 hr old at the time of serum removal were pre-R (did not divide). Of the cells older than 3 hr at serum removal, the likelihood that an individual cell was post-R increased with cell age before leveling off at about 7–10 hr (Figure 2B).

This observation that the timing of passage through R is variable contrasts with the results from similar serum removal experiments performed by the Zetterberg lab, which showed a sharp 3 hr cutoff for R in murine 3T3 cells (Figure 2 from Zetterberg and Larsson, 1991) and a similar 3 hr cutoff observed for whether 3T3 cells exhibit an additional 8 hr delay in re-entering the cell cycle following a transient serum removal (Figure 1 from Zetterberg

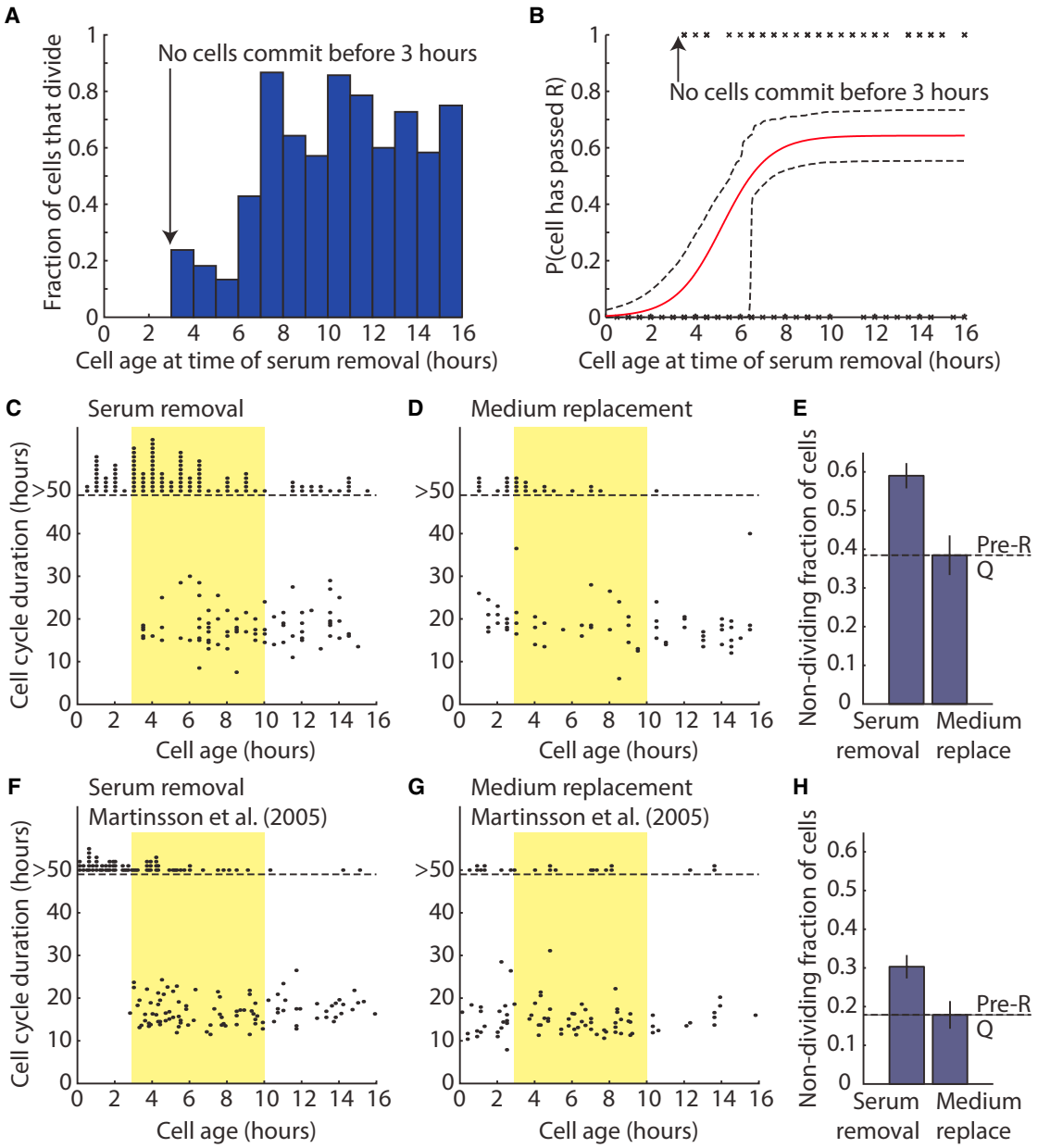

Figure 2. The Timing of Primary Fibroblast Passage through R Is Variable

(A) Fraction of HLFs that go on to divide following serum removal as a function of cell age at the time of serum removal (n = 268).

(B) Logistic regression estimate of the fraction of post-R HLFs from (A) as a function of cell age. Dashed lines represent 95% confidence interval based on bootstrap analysis of the data (see STAR Methods).

(C) Cell-cycle durations of individual cells plotted as a function of cell age at the time of serum removal (n = 268). Yellow region highlights cells with ages ≥3 and <10 hr at the time of serum removal.

(D) Cell-cycle durations of individual cells plotted as a function of cell age at the time of medium replacement (replotted from Figure S1E; n = 120).

(E) Fraction of cells within the yellow regions from (C) and (D) that fail to divide following serum removal or medium replacement (serum removal: 72/122 = 59%; medium replacement: 15/39 = 38%). Chi-square test p value = 0.025.

(F) Cell-cycle durations of individual cells plotted as a function of cell age at the time of serum removal (replotted from Martinsson et al., 2005; Figure 1B; n = 172).

(G) Cell-cycle durations of individual cells plotted as a function of cell age at the time of medium replace (replotted from Martinsson et al., 2005; Figure 1A; n = 103).

(H) Fraction of cells within the yellow regions from (F) and (G) that fail to divide following serum removal or medium replacement (serum removal: 30/99 = 30%; medium replacement: 10/56 = 18%). Chi-square test p value = 0.089.

and Larsson, 1985 and Figure 1 from Zetterberg and Larsson, 1991). In our experiments as well, it is striking that no cells younger than 3 hr old at the time of serum removal have passed R (Figure 2C). From those initial observations in 3T3 cells of a sharp cell-age-based difference in cell fates in response to transient or permanent serum removal, Zetterberg and colleagues defined R as taking place consistently at about 3 hr following division.

Our disagreement regarding the timing of R stems from how we interpret the cells that are older than 3 hr but do not divide after serum removal. Certainly, some of these cells are quiescent (Q) and so would not have divided even if serum levels were maintained, but others are potentially pre-R cells that would have gone on to divide if serum was not removed. To estimate the fraction of Q cells, we measured the fraction of cells 3–10 hr old that failed to divide in a control experiment in which the medium was replaced with serum-containing medium (Figure 2D). 38% of cells failed to divide, which gives us a baseline estimate that 38% of cells in these conditions will become quiescent after cell division (Figure 2E). However, when cells between the ages of 3 and 10 hr are exposed to serum removal, 59% fail to divide (Figure 2E). Thus, we estimate that of the cells that are 3–10 hr old, 38% were Q, 21% were pre-R, and 41% were post-R at the time of serum removal. When we perform the same analysis on the data from the serum removal experiments by Zetterberg and colleagues examining human diploid fibroblasts (Martinsson et al., 2005), we see a similar trend (Figures 2F–2H). Of cells between 3 and 10 hr old, we estimate that 18% were Q, 12% were pre-R, and 70% were post-R. Chi-square tests indicated that the pre-R fractions in each set of experiments were likely non-zero ($p < 0.05$ for our data). Indeed, the fraction of dividing cells increases with increasing cell ages from 3 to 10 hr (Figure S2). Taken together, both our data and those of Zetterberg and colleagues support a model where R is passed at a variable time between 3 and 10 hr after division in primary human fibroblasts.

A Cdk Activity Threshold Accurately Predicts Passage through R

Having established the timing of R within G1, we next sought to determine which molecular event corresponds to passage through R. The highly variable timing of R implies that even populations of cells synchronously released from a cell-cycle arrest will proceed through R at widely different times. This will then result in bulk biochemical measurements blurring together events preceding and following passage through R. In contrast, our single-cell assay allows us to determine whether each cell passed R by the time of serum removal. By measuring the change in fluorescent reporters of specific protein activities in single cells, we can determine which molecular events correspond to passage through R. Note that under our microscopy conditions, the expression of live-cell fluorescent sensors did not affect cell-cycle durations (Figures S3A–S3C).

Guided by the consensus molecular view of the G1/S transition that R corresponds to the activation of a positive feedback loop of cyclin-dependent kinase (Cdk) activity, Rb phosphorylation, and E2F-dependent transcription (Figure 3A), we first examined Cdk activity using a recently developed live-cell sensor (HDHB-EGFP) (Hahn et al., 2009). Increasing phosphorylation of this sensor through the cell cycle drives its export from the nucleus to the cytoplasm (Spencer et al., 2013) (Figure 3B). Thus, the ratio of cytoplasmic to nuclear fluorescence of HDHB-EGFP is a measure of cell-cycle phase. Its increase in primary cells begins in G1 and continues through the cell cycle (Figures 3C–3E and S3D).

To determine the relationship between Cdk activity and R, we measured the response of cells expressing HDHB-EGFP to serum removal (Figure 3F). Cdk activity at the time of serum removal was highly correlated with R (Figures 3G and 3H). Strikingly, a simple threshold model, where cells go on to divide if and only if their Cdk activity is above a threshold (cytoplasmic-to-nuclear HDHB-EGFP fluorescence ratio >0.84) at the time of serum removal, correctly predicted passage through R for 96% of the cells (Figures 3I and S3E). The threshold, chosen by logistic regression is the optimally predictive threshold (Figure S3F) and shows a good tradeoff between high true positive rate and low false positive rate as indicated by an ROC curve (Figure S3G). In sharp contrast, a threshold model using only cell age (time since previous cytokinesis) at the time of serum removal correctly predicted passage through R for only 61% of the cells (Figures S3H and S3I). Moreover, a linear model predicting passage through R using a combination of cell age and Cdk activity showed that the coefficient multiplying cell age was not significantly different from 0 ($p > 0.05$). Thus, while passage through R correlates with time since division, this can mostly be explained by cell-to-cell differences in Cdk activity. We therefore define R as the first increase in Cdk activity above this precise threshold. Strikingly, cells do not pass this threshold until after the 3 hr period identified as the earliest time that R can be passed (Figure S3J). That this threshold is far below the eventual maximum Cdk activity is consistent with previous studies showing that high levels of phospho-Rb, active E2F, and cyclin E were only observed several hours after R (Ekholm et al., 2001; Martinsson et al., 2005). Similarly, we previously found that commitment to cell division in budding yeast coincided with the onset, rather than the peak, of G1 cyclin transcription (Doncic et al., 2011).

Cell-Cycle-Dependent Activation of the E2F1 Promoter Coincides with R

Next, we aimed to determine the temporal relationship between R and the transcriptional activation of E2F1, which is central to G1/S positive feedback (Figure 3A). To monitor E2F1 transcriptional activation, we constructed a fluorescent reporter using a 796 base pair fragment upstream of the E2F1 transcription start site, which contains two known E2F-binding sites (Johnson et al., 1994; Yao et al., 2008). This promoter was used to drive expression of a destabilized, nuclear-localized EGFP (EGFP-PEST; see STAR Methods) (Figure 4A). Asynchronously growing HLFs containing the E2F1pr-EGFP-PEST reporter were monitored over multiple cell cycles. We identified the timing of transcriptional activation relative to the previous division by detecting an inflection point in the spline-fitted fluorescence signal (Eser et al., 2011) (Figures 4B and 4C). The mean time at which the E2F1 promoter is activated is not significantly different from the mean time at which Cdk activity crosses the threshold for R (t test, p value = 0.31; Figure 4D). We do note the larger

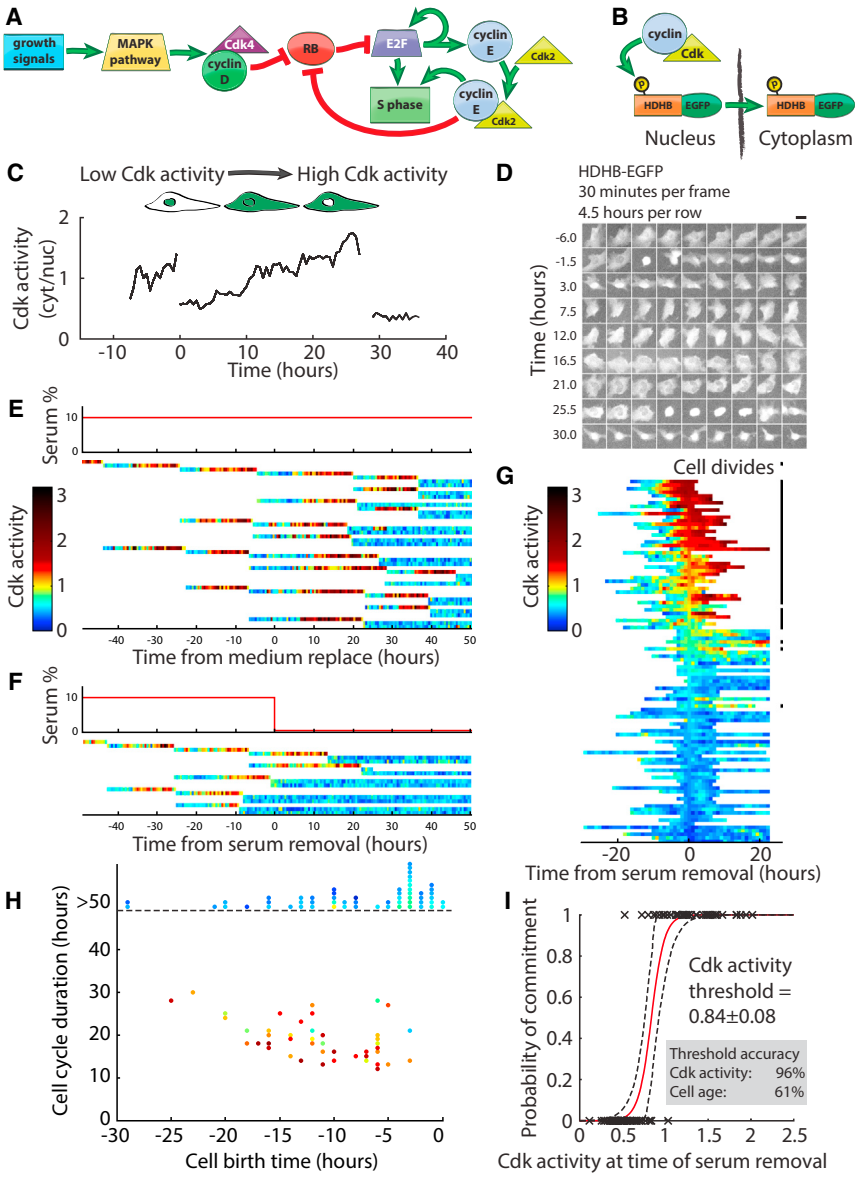

Figure 3. A Cdk Activity Threshold Accurately Predicts Passage through R

(A) Schematic of mammalian G1/S regulatory network.

(B) Schematic of HDHB-EGFP Cdk activity sensor. As HDHB-EGFP is increasingly phosphorylated over the course of the cell cycle, it translocates from the nucleus to the cytoplasm.

(C) Example single-cell traces of Cdk activity. Cdk activity was measured as the ratio of median cytoplasmic to median nuclear HDHB-EGFP fluorescence (cyt/nuc).

(D) Fluorescence images from the traces measured in (C) at 30 min time points. Scale bar represents 30 μm.

(E) Traces from a lineage of cells exposed to a medium replace control at time 0. At the end of the experiment, contact inhibition prevents further divisions.

(F) Traces from a lineage of cells exposed to serum removal at time 0. Cells with high Cdk activity at the time of serum removal (the top two rows at time 0) go on to divide, while cells with low Cdk activity at that time arrest (the bottom six rows at time 0).

(G) Each row is a Cdk activity trace for an individual cell (n = 102). Rows are ordered by Cdk activity at the time of serum removal. Cells that divide after serum removal are marked with a black square to the right of the trace. Note that all cells that did not divide were tracked at least 24 hr following serum removal but were not necessarily segmented for that entire period.

(H) A commitment plot (as in Figure 1G) in which each cell from (G) is colored based on its Cdk activity at the time of serum removal using the same scale as in (E)–(G).

(I) Logistic regression estimating the probability a cell was committed to division as a function of its Cdk activity at the time of serum removal. The Cdk activity threshold of 0.84 was calculated from the midpoint of the logistic regression (95% confidence interval from bootstrap analysis: 0.76–0.93). Inset: accuracy of threshold models based on cell age or Cdk activity (see STAR Methods).

variability in the timing of E2F1 promoter activation, but we are unsure if this reflects natural variation in the timing of E2F1 activation, noise in measurements, or noise in analysis of the reporter. Recently, it was shown that expression from a similar E2F1 promoter fragment correlated with the onset of S phase (Dong et al., 2014). In that study, the threshold amplitude for S was only a fraction of the maximum expression of E2F1, which is consistent with our results showing that R coincides with the activation of E2F1 expression rather than the maximum. Taken together, these data support a model where the activation of the E2F1 promoter and attainment of a threshold level of Cdk activity correspond to passage through R.

R Occurs 1–2 hr before S Phase

Next, we determined the timing of R relative to the onset of S phase. To measure the timing of S phase onset, we used the FUCCI geminin reporter (Sakaue-Sawano et al., 2008). The first appearance of geminin-GFP occurs due to the inactivation of APC/C^{Cdh1} and is coincident with the initiation of S phase (Sakaue-Sawano et al., 2008) (Figure 4E). We measured geminin-GFP levels in asynchronously cycling HLFs to determine the amount of time between the previous division and the beginning of S phase. When we compare this distribution to the distribution of times between division and reaching the Cdk activity threshold for R, we see that the distributions are similar but that the S phase entry distribution is delayed by 2 hrs (Figure 4D). To test the hypothesis that entry into S phase follows R by a consistent 2 hr interval, we compared the distribution of Cdk threshold times with the distribution of S phase entry times minus 2 hr and found that the distributions were similar (KS test, $p > 0.29$; Figure S4A). We also measured the timing of Cdk activation and S phase entry in HLFs expressing both

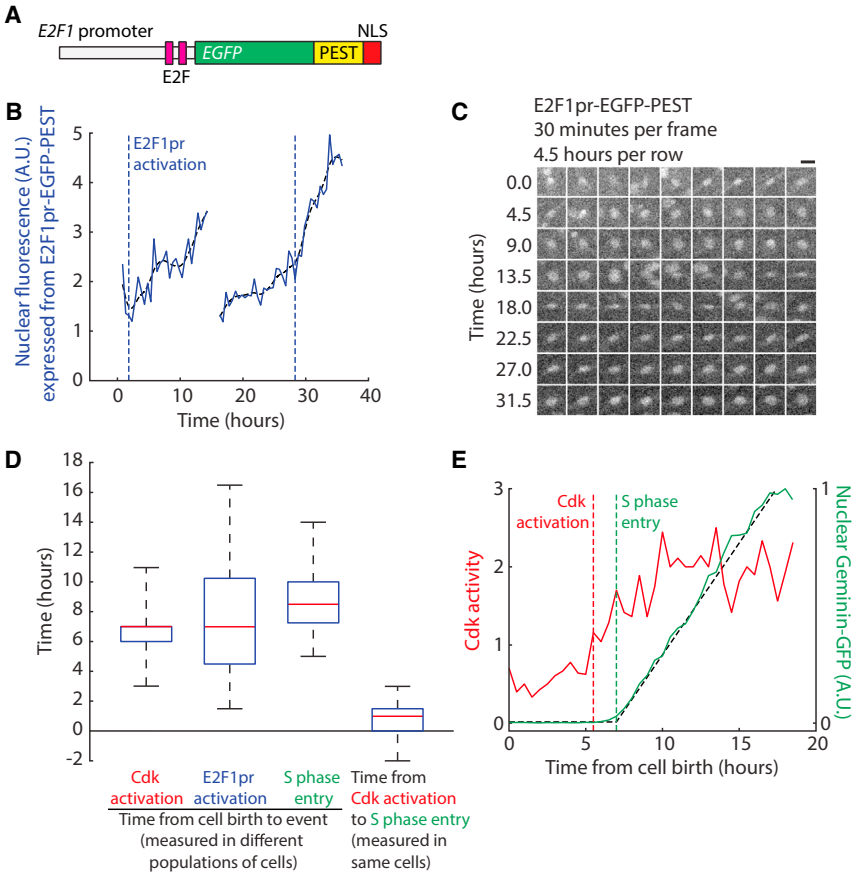

Figure 4. Cell-Cycle-Dependent Activation of the E2F1 Promoter Coincides with R, Which Occurs 1–2 hr before S Phase

(A) Schematic of E2F1pr-EGFP-PEST fluorescent reporter.

(B) Example traces from a cell expressing E2F1pr-EGFP-PEST (blue). Dashed lines denote *E2F1* transcriptional activation, which is calculated as the maximum of the second derivative of a spline fit of the trace (red; see STAR Methods).

(C) Fluorescence images from the traces measured in (B) at 30 min time points. Scale bar represents 30 μm.

(D) Boxplots summarizing the distributions of the times from cell birth to the Cdk activity commitment threshold (n = 30), activation of *E2F1* transcription (n = 25), or S phase (n = 52) from populations of cells expressing one of the following constructs: HDHB-EGFP, E2F1pr-EGFP-PEST, or geminin-GFP. Also shown is a boxplot summarizing the distribution of S phase entry times minus Cdk activation times from cells expressing both HDHB-mCherry and geminin-GFP. Red bars indicate medians, blue boxes indicate 25th and 75th percentiles (for Cdk activation, both the median and the 75th percentile are 7 hr), and bars indicate the most extreme values.

(E) Example traces from a cell expressing HDHB-mCherry and geminin-GFP. Cdk activation time is the first time point >0.84 followed by another time point >0.84. S phase entry time is determined by fitting the data to two lines and identifying the intersection.

HDHB-mCherry and geminin-GFP (Figures 4E and S4B). In these cells, S phase entry followed Cdk activation by approximately 1 hr. Taken together, our data support a model where variability in G1 length is almost entirely due to variability in the pre-R period and that entry into S phase follows R by about 1–2 hr.

Cells Commit at a Lower Cdk Activity Threshold in Response to MEK Inhibition

So far, we have shown that R in response to abrupt serum removal is precisely defined by Cdk activity. However, serum is a complex mixture stimulating several proliferation-promoting pathways, including the mitogen-activated protein kinase (MAPK) pathway. To determine the contribution of MAPK signaling to the Cdk activity threshold, we performed a variation of our commitment point assay (Figure 5A). Instead of removing serum, we inhibited MAPK pathway activity in the presence of serum. Since MAPK activity is essential for primary cell proliferation, this experiment allows us to identify the specific contribution of MAPK activity to commitment. To inhibit the MAPK pathway, we use 500 nM PD0325901, which specifically inhibits the pathway component MEK (Bain et al., 2007) (Figures S5A–S5E). Cdk activity at the time of MEK inhibitor addition was predictive of whether each cell was committed to division (Figures 5B and 5C). However, the threshold Cdk activity was lower than that defining R in response to serum removal (Figure 5D; MEK inhibition Cdk activity threshold = 0.68 ± 0.10 versus 0.84 ± 0.08 for serum removal; 95% confidence interval from bootstrapped data; $p < 0.01$). The threshold was also less predictive than the threshold determined from the serum removal experiments (Figures S5F and S5G). When MEK alone is inhibited, less Cdk activity is required for a cell to be committed to division than when serum is removed completely. These results are consistent with a model in which commitment to division is due to a combination of upstream growth factor-dependent signals and downstream positive feedback activation. In comparison with serum removal, MEK inhibition removes some, but not all, upstream signals. The maintenance of some upstream proliferative signaling then results in a lower requirement for downstream Cdk-positive feedback to commit cells to division.

Since Cdk activity drives the positive feedback loop controlling proliferation, we attempted to perturb its dynamics in HLFs by exposing them to varying concentrations of the Cdk2 inhibitor roscovitine (Meijer et al., 1997). The population-wide rate of proliferation decreased with increasing roscovitine concentration (Figure S5H). However, we saw a bimodal response at the single-cell level. Cells either proceeded through the cell division cycle with nearly normal kinetics or died (Figures S5I and S5J), implying that we were unable to perturb R using roscovitine without inducing other cellular responses. Similarly, a recent study found that a different Cdk2 inhibitor, CVT-313, also induced a bimodal proliferative response (Dong et al., 2014).

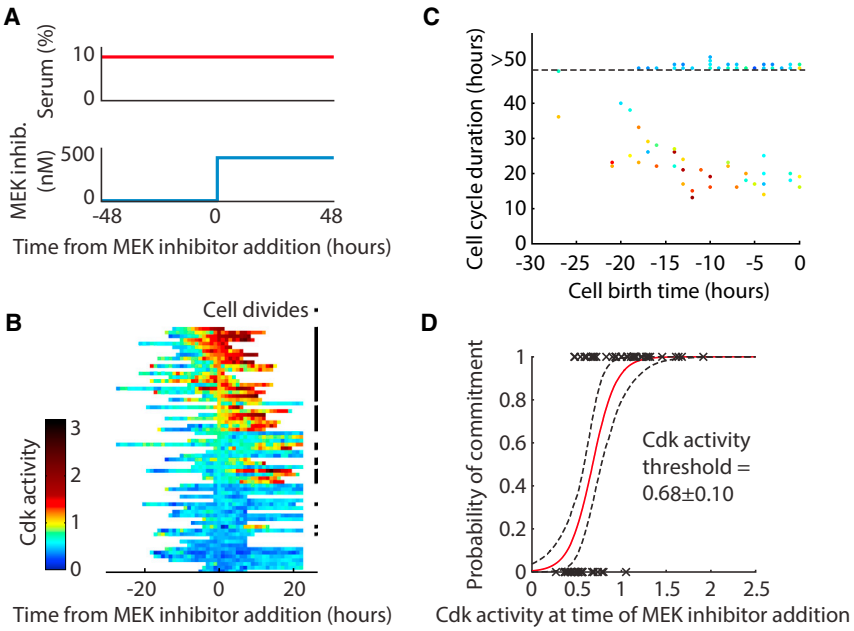

Figure 5. Cells Commit at a Lower Cdk Activity Threshold in Response to MEK Inhibition

(A) Experiment schematic: asynchronous HLFs expressing HDHB-EGFP were treated with 500 nM MEK inhibitor (PD0325901) while grown in constant 10% serum.

(B) Each row is a Cdk activity trace for an individual cell (n = 66). Rows are ordered by Cdk activity at the time of MEK inhibitor addition. Cells that divide after serum removal are marked with a black square to the right of the trace. Note that all cells that did not divide were tracked at least 24 hr following MEK inhibition but were not necessarily segmented for that entire period.

(C) A commitment plot (as in Figure 3H) in which each cell is colored based on its Cdk activity at the time of MEK inhibitor addition using the same scale as in (B).

(D) Logistic regression estimating the probability a cell was committed to division as a function of its Cdk activity at the time of MEK inhibitor addition. The Cdk activity threshold of 0.68 was calculated from the midpoint of the logistic regression (95% confidence interval from bootstrap analysis: 0.59–0.79). The Cdk activity threshold for commitment in response to MEK inhibition is significantly lower than the threshold in response to serum removal (0.68 versus 0.84; $p < 0.01$).

HDHB-EGFP Likely Senses the Activity of Multiple Cyclin-Cdk Complexes

The HDHB-based sensor is strikingly predictive of cell fate in response to serum removal, but it is not clear exactly what it is measuring. The full-length HDHB protein is exported from the nucleus to the cytoplasm over the course of the cell cycle (Gu et al., 2004). This translocation is mediated by a C-terminal cluster of Cdk-consensus phosphorylation sites from 957 to 1,087. An HDHB fragment containing these Cdk sites fused to GFP is sufficient to reproduce the cell-cycle-dependent translocation (Gu et al., 2004). This fragment was further truncated to amino acids 994–1,087 to make the HDHB fragment used here (Hahn et al., 2009). We note that another recently reported Cdk activity sensor is based on the full 957–1,087 C-terminal region originally identified by Gu et al. (2004) and has slightly different dynamics, including a distinctive local peak in activity at the G1/S transition (Barr et al., 2016).

The phosphorylation-dependent localization of the shorter HDHB fragment we use was described as Cdk2 specific on the basis of two sets of experiments (Spencer et al., 2013). First, the sensor's activity dropped to baseline upon addition of 10 μM "Cdk1/2i" (EMD Biosciences #217714) but did not change upon addition of 9 μM "Cdk1i" (RO-3306). However, at these concentrations *in vitro*, both of these molecules should inhibit Cdk1 and Cdk2 in addition to other kinases (Lin et al., 2005; Vassilev et al., 2006). This makes the interpretation of these inhibitor-based experiments difficult. Second, a series of kinase assays showed specific phosphorylation of the purified HDHB fragment by E1-Cdk2 and A2-Cdk2, but not by B1-Cdk1, D1-Cdk4, or D1-Cdk6 (Spencer et al., 2013). This experiment confirms that two different cyclin-Cdk2 complexes can phosphorylate the HDHB fragment, but does not exclude the possibility that other untested cyclin-Cdk complexes or other kinases could phosphorylate it as well.

The specificity of cyclin-Cdk complexes is generally thought to come from the cyclin rather than from the Cdk subunit (Morgan, 2007). It is therefore likely that the sensor is specific to cyclins E and A rather than to Cdk2. This view is supported by experiments involving siRNA targeting cyclins E and A (Spencer et al., 2013). When cyclins E1 and E2 are targeted, the sensor activity remains low. When cyclin A2 is targeted, the sensor begins to rise but reaches a plateau below the peak level (Spencer et al., 2013). These experiments, combined with previous observations that Cdk1 also forms complexes with cyclins E and A (Aleem et al., 2005; Koff et al., 1991; Merrick et al., 2011; Welcker and Clurman, 2005), suggest that the sensor may be measuring an aggregate of cyclin E- and A-dependent Cdk2 and Cdk1 activities (Figure 6A).

To test this hypothesis, we first sought to test the ability of a variety of cyclin-Cdk fusions to phosphorylate the HDHB sensor *in vitro*. We performed *in vitro* kinase assays with the following cyclin-Cdk fusions: cyclin D1-Cdk4, cyclin E1-Cdk2, cyclin E1-Cdk1, cyclin A2-Cdk2, cyclin A2-Cdk1, cyclin B1-Cdk2, and cyclin B1-Cdk1 (see STAR Methods). Cyclin E1-Cdk1 and cyclin A2-Cdk1 both phosphorylate HDHB-EGFP about as strongly as cyclin E1-Cdk2 and cyclin A2-Cdk2, respectively (Figure 6B). We also confirmed the previously reported lack of phosphorylation of HDHB-EGFP by cyclin D1-Cdk4 (Spencer et al., 2013) and showed that cyclin B1-Cdk2 and cyclin B1-Cdk1 poorly phosphorylate HDHB-EGFP. These *in vitro* experiments, combined with the cyclin E and A siRNA experiments from Spencer et al. (2013), suggest that both Cdk2 and Cdk1 in complex with either cyclin E or cyclin A play a role in the phosphorylation and localization of the HDHB-EGFP Cdk activity sensor.

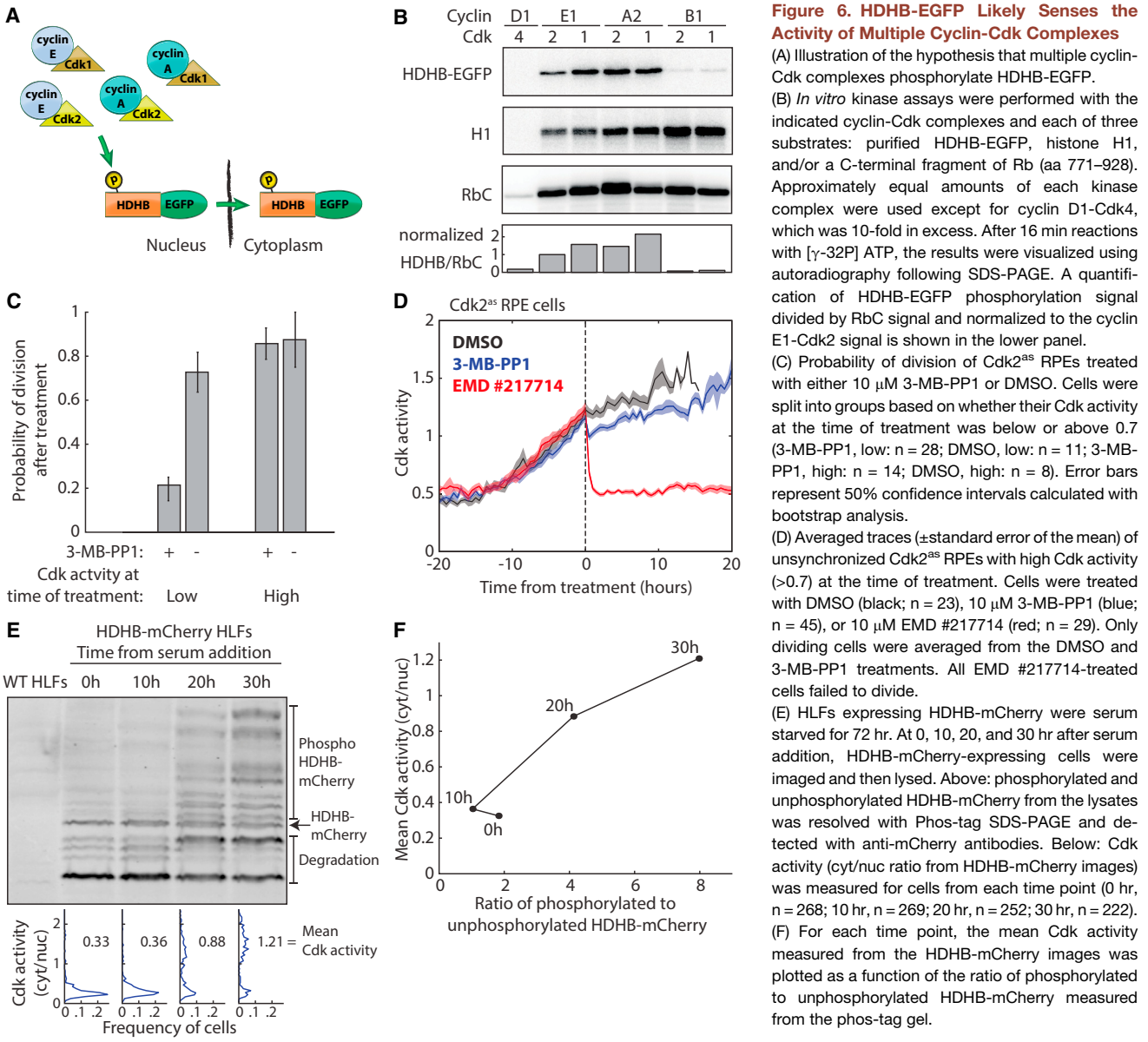

Figure 6. HDHB-EGFP Likely Senses the Activity of Multiple Cyclin-Cdk Complexes

(A) Illustration of the hypothesis that multiple cyclin-Cdk complexes phosphorylate HDHB-EGFP.

(B) *In vitro* kinase assays were performed with the indicated cyclin-Cdk complexes and each of three substrates: purified HDHB-EGFP, histone H1, and/or a C-terminal fragment of Rb (aa 771–928). Approximately equal amounts of each kinase complex were used except for cyclin D1-Cdk4, which was 10-fold in excess. After 16 min reactions with [γ-32P] ATP, the results were visualized using autoradiography following SDS-PAGE. A quantification of HDHB-EGFP phosphorylation signal divided by RbC signal and normalized to the cyclin E1-Cdk2 signal is shown in the lower panel.

(C) Probability of division of Cdk2^{as} RPEs treated with either 10 μM 3-MB-PP1 or DMSO. Cells were split into groups based on whether their Cdk activity at the time of treatment was below or above 0.7 (3-MB-PP1, low: n = 28; DMSO, low: n = 11; 3-MB-PP1, high: n = 14; DMSO, high: n = 8). Error bars represent 50% confidence intervals calculated with bootstrap analysis.

(D) Averaged traces (±standard error of the mean) of unsynchronized Cdk2^{as} RPEs with high Cdk activity (>0.7) at the time of treatment. Cells were treated with DMSO (black; n = 23), 10 μM 3-MB-PP1 (blue; n = 45), or 10 μM EMD #217714 (red; n = 29). Only dividing cells were averaged from the DMSO and 3-MB-PP1 treatments. All EMD #217714-treated cells failed to divide.

(E) HLFs expressing HDHB-mCherry were serum starved for 72 hr. At 0, 10, 20, and 30 hr after serum addition, HDHB-mCherry-expressing cells were imaged and then lysed. Above: phosphorylated and unphosphorylated HDHB-mCherry from the lysates was resolved with Phos-tag SDS-PAGE and detected with anti-mCherry antibodies. Below: Cdk activity (cyt/nuc ratio from HDHB-mCherry images) was measured for cells from each time point (0 hr, n = 268; 10 hr, n = 269; 20 hr, n = 252; 30 hr, n = 222).

(F) For each time point, the mean Cdk activity measured from the HDHB-mCherry images was plotted as a function of the ratio of phosphorylated to unphosphorylated HDHB-mCherry measured from the phos-tag gel.

In order to determine the relative importance of Cdk2 activity to the sensor's localization, we decided to examine a retinal pigmented epithelium cell line in which both copies of Cdk2 have been replaced by analog-sensitive alleles of Cdk2 (Cdk2^{as} RPEs) (Merrick et al., 2011). This allowed us to acutely and specifically inhibit Cdk2 without the nonspecific effects of other small-molecule inhibitors. We expressed HDHB-EGFP in Cdk2^{as} RPEs and performed an experiment where, after 2 days, cells were treated with either the ATP analog 3-MB-PP1 dissolved in DMSO or a DMSO control. Consistent with a role for Cdk2 in R, cells with low Cdk activity (<0.7) were less likely to build up Cdk activity and divide if they were treated with analog, whereas cells with high Cdk activity (>0.7) were equally likely to divide if treated with analog or DMSO (Figure 6C).

To determine how specific Cdk2 inhibition affects sensor localization, we averaged sensor traces for cells that had high activity at the time of analog treatment. The drop in Cdk activity in these cells immediately following analog addition indicates that only 25% of the above-background activity is due to Cdk2 in these cells (Figure 6D, blue). In contrast, the addition of 10 μM EMD #217714 (as in Spencer et al., 2013) results in an immediate drop in sensor activity to baseline and no subsequent cell division (Figure 6D, red). This baseline level is independent of cell-cycle position before EMD#217714 treatment, suggesting that other cell-cycle-dependent kinases not inhibited by EMD#217714 do not participate in HDHB-EGFP localization (Figure S6A). Wild-type cells show no similar drop in sensor activity upon analog addition (Figure S6B), and the addition of a molecule stabilizing cyclin E-Cdk2 binding in Cdk2^{as} RPE cells,

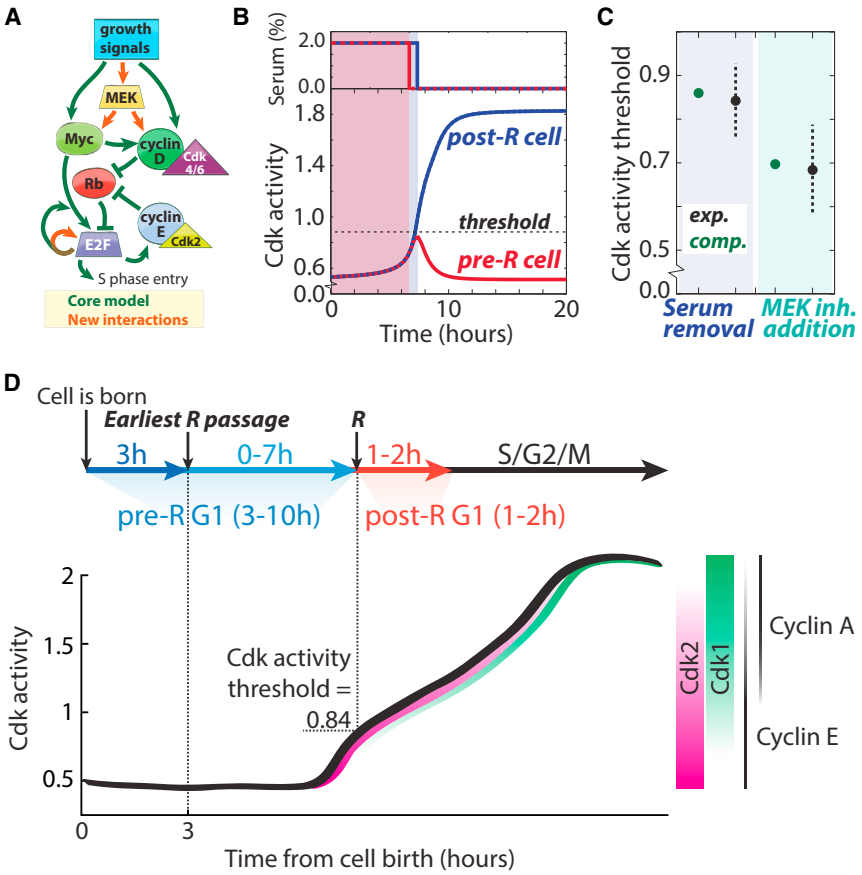

Figure 7. A Differential Equation Model of R Is Consistent with Measured Cdk Activity Thresholds

(A) Schematic indicating molecular interactions included in the model adapted from Yao et al., 2008 (see STAR Methods). MEK-dependent growth factor signals and a serum-independent E2F synthesis term were added (orange) to the interactions in the previously existing model (green).

(B) Serum was removed from the model after various amounts of time in order to simulate the serum removal experiments from Figures 3F and 3G. Example traces show dynamics for cells that were pre-R (red) and post-R (blue) at the time of serum removal.

(C) Experimental and computational commitment thresholds in response to serum removal and MEK inhibition. Growth factor proliferative signaling in response to serum is decomposed into MEK-independent and MEK-dependent fractions.

(D) Schematic of Cdk activity (cyt/nuc HDHB ratio) changes over the course of the cell cycle in primary human lung fibroblasts.

6-BAP (Merrick et al., 2011), did not affect the results (Figures S6C—S6E).

In summary, we found that Cdk2 activity is important for the initial rise of the sensor and for cell-cycle commitment. However, Cdk2 activity alone is not sufficient to explain subsequent rise in sensor activity. Our experiments, in combination with the siRNA experiments from Spencer et al. (2013), suggest a model where the phosphorylation and localization of the HDHB-based Cdk activity sensor depends most strongly on cyclin E-Cdk2 activity during the time leading up to R and subsequently on a combination of cyclin E-Cdk2, cyclin E-Cdk1, cyclin A-Cdk2, and cyclin A-Cdk1 activities.

HDHB-Based Sensor Phosphorylation Correlates with Cdk Activity Measurements *In Vivo*

Having established that the localization of an HDHB-based sensor predicts R, and that this sensor is phosphorylated *in vitro* by Cdk1 and Cdk2 in complex with either cyclin E or cyclin A, we next set out to test whether sensor localization and phorphorylation status were correlated *in vivo*. To test this, HLFs expressing HDHB-mCherry were serum starved for 72 hr. After serum addition, dishes of cells were imaged for HDHB-mCherry localization and then lysed. Phosphorylated and unphosphorylated HDHB-mCherry was resolved from the lysates using Phos-tag SDS-PAGE with an antibody against mCherry (Figure 6E). The identification of phosphorylated and unphosphorylated bands was determined using a phosphatase assay (Figure S6F). As the cells re-entered the cell cycle after release from serum starvation, the phosphorylation of HDHB-mCherry increased alongside the microscopy-based measurements of Cdk activity (Figure 6F). This experiment supports the use of the HDHB-based sensor to measure cyclin-Cdk complex activity *in vivo*.

A Differential Equation Model of R Is Consistent with Measured Cdk Activity Thresholds

Having performed a quantitative experimental analysis of R using the Cdk activity sensor, and having characterized the sensor's cyclin-Cdk specificity, we next sought to incorporate our findings into the most established ordinary differential equation model of R (Yao et al., 2008) (Figure 7A). We used this model to simulate our experiments by providing serum for variable amounts of time, removing it, and observing the system dynamics. Our experimental results show that once Cdk activity rises above a threshold, it will remain high even if serum is removed. However, in the model of Yao et al., Cdk activity falls back to baseline if serum levels drop to zero (Figure S7A). To bring the model in line with our experimental results showing cell-cycle progression following serum removal, we added a serum-independent source of E2F1 synthesis (Leung et al., 2008) (Figures 7A, 7B, and S7B). Next, we sought to incorporate our result that the threshold for commitment in response to MEK inhibition was distinct from the threshold for commitment in response to serum removal. Since serum stimulation activates MAPK and other proliferative signaling pathways, we separated the serum term in the equations into MAPK-dependent and MAPK-independent contributions (Figure 7A). By specifying

the MAPK-dependent fraction of serum-induced proliferative signaling, we fit our two distinct thresholds (Figure 7C). Thus, following two important modifications, our quantitative measurements were easily incorporated into the prevailing differential equations model.

DISCUSSION

Our work helps to reconcile several counterintuitive sets of studies about the restriction point with the consensus view of G1/S control in mammalian cells. Our model describes the restriction point in primary fibroblasts as being associated with the activation of a positive feedback loop of Cdk activity, E2F-dependent transcription, and Rb hyperphosphorylation. Zetterberg and colleagues claimed that these molecular events could not define R on the basis of time-lapse microscopy experiments followed by immunofluorescence in HDFs, which showed that events like Rb phosphorylation (Martinsson et al., 2005) and cyclin E accumulation (Ekholm et al., 2001) occurred after the 3–4 hr time point they associated with R. However, our experiments with primary HLFs and our reanalysis of the HDF data from Martinsson et al. (2005) suggest that the timing of R is more variable in these cell types than in the mouse 3T3 cells in which that 3–4 hr time point was originally defined (Zetterberg and Larsson, 1985, 1991). Although 3 hr is the earliest time at which our primary cells were observed to pass R, the fraction of cells that had passed R increased with cell age from 3 to 10 hr (Figures 2A, 2B, and S2C). This timing of R also matches the timing at which individual HLFs pass the threshold level of Cdk activity required to be committed to division (Figure 4C) and to the timing of cyclin E accumulation in the HDFs of Ekholm et al. (Figure 4 in Ekholm et al., 2001). Additionally, the fact that peak levels of Rb phosphorylation were not seen in individual cells until well after the 3–4 hr time point (Martinsson et al., 2005) makes sense, given that the point of commitment is at the induction of the positive feedback loop, at low levels of Cdk activity. Maximal activation, including complete hyperphosphorylation of Rb, may not occur until hours later. Thus, the HDF data from the Zetterberg Lab are consistent with R in primary fibroblasts occurring at a variable time 3–10 hr into the cell cycle alongside the onset of positive feedback loop activation (Figure 7D). Recent work has found that a large fraction of the variability in the timing of the pre-R period can be accounted for by DNA damage in the previous cell cycle (Arora et al., 2017; Barr et al., 2017).

Another contribution of our work to the field of mammalian G1/S control is our clarification of the specificity of the increasingly widely used HDHB-based Cdk activity sensor. This sensor has been reported as specific to Cdk2 activity (Spencer et al., 2013), and subsequent works have also referred to it as Cdk2 specific (Arora et al., 2017; Barr et al., 2016, 2017; Cappell et al., 2016; Yang et al., 2017). However, this is unlikely because cyclin-Cdk specificity is generally determined by the cyclin subunit rather than the Cdk subunit (Morgan, 2007). The cyclin E and A specificity of the sensor has been determined by siRNA experiments (Barr et al., 2016; Spencer et al., 2013). However, both Cdk2 and Cdk1 have also been shown to bind cyclins E and A, suggesting that Cdk1 in complex with those cyclins may also play a role in the sensor's localization (Aleem et al., 2005; Koff et al., 1991; Merrick et al., 2011; Morgan, 2007; Welcker and Clurman, 2005). Consistent with this picture, our work shows that Cdk2 is not responsible for all sensor activity *in vivo* and that Cdk1 in complex with either cyclin E or cyclin A can phosphorylate the HDHB-EGFP sensor *in vitro*. When taken in combination with our other results, this suggests that the HDHB-based Cdk activity sensor's initial rise above baseline depends on cyclin E-Cdk2 and that its subsequent increase depends on a mix of activities from Cdk1 and Cdk2 in complex with cyclins E and A (Figure 7D).

Our model also describes the timing of R in primary cells as occurring in G1 1–2 hr before DNA replication, consistent with an earlier estimate from population data (Yen and Pardee, 1978). This contrasts with a recent study that cast doubt on the G1 R model by showing that some cell lines commit to division prior to the mitosis of the previous cell cycle (Spencer et al., 2013). These disparate observations can be reconciled by the fact that G1 R is frequently lost in immortalized, transformed, or cancerous cell lines (Campisi et al., 1982; Yen and Pardee, 1978; Zetterberg et al., 1995). Indeed, overactive proliferative signaling is a noted hallmark of cancer (Hanahan and Weinberg, 2011).

In response to serum removal or MAPK inhibition, two anti-proliferative perturbations, cells with Cdk activity above specific thresholds are committed to division. However, the two thresholds are different. Thus, distinct anti-proliferative perturbations may each have their own threshold, a result which naturally arises from the analysis of positive feedback network architectures (Doncic et al., 2011; Justman et al., 2009). In positive feedback networks, commitment results from both upstream input signals and downstream positive feedback. The more the upstream signal is reduced, the greater the requirement for positive feedback activity to commit. Thus, we expect that a continuum of different commitment thresholds can arise from the same positive feedback network depending on the magnitude of the reduction in upstream signaling activities. In the context of other cell types, we expect upstream signaling pathways to have different activities, so that the commitment threshold would likely be different even in identical conditions. Our work suggests that in any particular cell type and condition, we may be able to determine a highly predictive Cdk activity threshold. However, the thresholds determined here may not be the most predictive in other conditions or cell types.

Just as we here showed that Cdk activity accurately predicted R, we previously showed that Cdk activity accurately predicted division in budding yeast (Doncic et al., 2011). In each case, the regulatory networks are composed of several interconnected signaling pathways. This network complexity in combination with the widespread cell-to-cell variation in protein concentrations led us to expect that measurements of many molecular events would be required to predict division (Atay and Skotheim, 2014; Raj and van Oudenaarden, 2008). Yet single measurements sufficed. This demonstrates that the states of even highly complex decision-making networks can be accurately determined with single measurements.

STAR★METHODS

Detailed methods are provided in the online version of this paper and include the following:

- KEY RESOURCES TABLE
- CONTACT FOR REAGENT AND RESOURCE SHARING
- EXPERIMENTAL MODEL AND SUBJECT DETAILS
  - Cell line and primary cell culture
- METHOD DETAILS
  - Fluorescent reporters
  - Microscopy
  - Image analysis
  - Transcriptional activation analysis
  - Cdk activity threshold analysis
  - Protein expression and purification
  - *In vitro* kinase assay
  - Phos-tag SDS-PAGE and phosphatase assay
  - Prediction framework
  - FACS analysis
  - ODE model of R
- QUANTIFICATION AND STATISTICAL ANALYSIS

SUPPLEMENTAL INFORMATION

Supplemental Information includes seven figures and can be found with this article online at https://doi.org/10.1016/j.molcel.2017.12.017.

ACKNOWLEDGMENTS

We thank Matthew Storm Bull for participating in the initial analysis of E2F1 transcription timing, Karina Castillo and Alexander Velasquez for participating in cell tracking analysis, and Joe Lipsick and Rob de Bruin for insightful comments on the manuscript. We thank the Santos Lab (UMDNJ), Stearns Lab (Stanford), Cleveland Lab (UCSD), Khavari Lab (Stanford), Fisher Lab (Mount Sinai), and Harbury Lab (Stanford) for sharing the indicated cell lines. This work was supported by a Burroughs Wellcome Fund Career Award at the Scientific Interface, the NIH through R01 GM092925 and T32 GM007276 (A.J. and C.S.), and a Human Science Frontier Program postdoctoral fellowship (M.K.).

AUTHOR CONTRIBUTIONS

C.S., A.J., and J.M.S. designed the study. C.S., A.J., E.Z., and C.J.K. performed and analyzed live-cell imaging experiments; M.K. performed *in vitro* kinase assays; E.Z. performed phosphatase assays; C.S. and A.D. developed imaging analysis tools and mathematical models; and C.S., A.D., and J.M.S. wrote the manuscript.

DECLARATION OF INTERESTS

The authors declare no competing interests.

Received: May 23, 2017
Revised: November 28, 2017
Accepted: December 19, 2017
Published: January 18, 2018

REFERENCES

Adams, P.D., Li, X., Sellers, W.R., Baker, K.B., Leng, X., Harper, J.W., Taya, Y., and Kaelin, W.G., Jr. (1999). Retinoblastoma protein contains a C-terminal motif that targets it for phosphorylation by cyclin-cdk complexes. Mol. Cell. Biol. *19*, 1068–1080.

Aleem, E., Kiyokawa, H., and Kaldis, P. (2005). Cdc2-cyclin E complexes regulate the G1/S phase transition. Nat. Cell Biol. *7*, 831–836.

Arora, M., Moser, J., Phadke, H., Basha, A.A., and Spencer, S.L. (2017). Endogenous replication stress in mother cells leads to quiescence of daughter cells. Cell Rep. *19*, 1351–1364.

Atay, O., and Skotheim, J.M. (2014). Modularity and predictability in cell signaling and decision making. Mol. Biol. Cell *25*, 3445–3450.

Bain, J., Plater, L., Elliott, M., Shpiro, N., Hastie, C.J., McLauchlan, H., Klevernic, I., Arthur, J.S.C., Alessi, D.R., and Cohen, P. (2007). The selectivity of protein kinase inhibitors: a further update. Biochem. J. *408*, 297–315.

Barr, A.R.R., Heldt, F.S.S., Zhang, T., Bakal, C., and Novák, B. (2016). A dynamical framework for the all-or-none G1/S transition. Cell Syst. *2*, 27–37.

Barr, A.R., Cooper, S., Heldt, F.S., Butera, F., Stoy, H., Mansfeld, J., Novák, B., and Bakal, C. (2017). DNA damage during S-phase mediates the proliferation-quiescence decision in the subsequent G1 via p21 expression. Nat. Commun. *8*, 14728.

Campisi, J., Medrano, E.E., Morreo, G., and Pardee, A.B. (1982). Restriction point control of cell growth by a labile protein: evidence for increased stability in transformed cells. Proc. Natl. Acad. Sci. USA *79*, 436–440.

Cappell, S.D., Chung, M., Jaimovich, A., Spencer, S.L., and Meyer, T. (2016). Irreversible APCCdh1 inactivation underlies the point of no return for cell-cycle entry. Cell *166*, 167–180.

Chytil, A., Waltner-Law, M., West, R., Friedman, D., Aakre, M., Barker, D., and Law, B. (2004). Construction of a cyclin D1-Cdk2 fusion protein to model the biological functions of cyclin D1-Cdk2 complexes. J. Biol. Chem. *279*, 47688–47698.

Coats, S., Flanagan, W.M., Nourse, J., and Roberts, J.M. (1996). Requirement of p27Kip1 for restriction point control of the fibroblast cell cycle. Science *272*, 877–880.

Corish, P., and Tyler-Smith, C. (1999). Attenuation of green fluorescent protein half-life in mammalian cells. Protein Eng. *12*, 1035–1040.

Doncic, A., and Skotheim, J.M. (2013). Feedforward regulation ensures stability and rapid reversibility of a cellular state. Mol. Cell *50*, 856–868.

Doncic, A., Falleur-Fettig, M., and Skotheim, J.M. (2011). Distinct interactions select and maintain a specific cell fate. Mol. Cell *43*, 528–539.

Doncic, A., Eser, U., Atay, O., and Skotheim, J.M. (2013). An algorithm to automate yeast segmentation and tracking. PLoS ONE *8*, e57970.

Doncic, A., Atay, O., Valk, E., Grande, A., Bush, A., Vasen, G., Colman-Lerner, A., Loog, M., and Skotheim, J.M. (2015). Compartmentalization of a bistable switch enables memory to cross a feedback-driven transition. Cell *160*, 1182–1195.

Dong, P., Maddali, M.V., Srimani, J.K., Thélot, F., Nevins, J.R., Mathey-Prevot, B., and You, L. (2014). Division of labour between Myc and G1 cyclins in cell cycle commitment and pace control. Nat. Commun. *5*, 4750.

Ekholm, S.V.S., Zickert, P., Reed, S.I., and Zetterberg, A. (2001). Accumulation of cyclin E is not a prerequisite for passage through the restriction point. Mol. Cell. Biol. *21*, 3256–3265.

Eser, U., Falleur-Fettig, M., Johnson, A., and Skotheim, J.M. (2011). Commitment to a cellular transition precedes genome-wide transcriptional change. Mol. Cell *43*, 515–527.

Foster, D.A., Yellen, P., Xu, L., and Saqcena, M. (2010). Regulation of G1 cell cycle progression: distinguishing the restriction point from a nutrient-sensing cell growth checkpoint(s). Genes Cancer *1*, 1124–1131.

Geng, Y., Eaton, E.N., Picón, M., Roberts, J.M., Lundberg, A.S., Gifford, A., Sardet, C., and Weinberg, R.A. (1996). Regulation of cyclin E transcription by E2Fs and retinoblastoma protein. Oncogene *12*, 1173–1180.

Gu, J., Xia, X., Yan, P., Liu, H., Podust, V.N., Reynolds, A.B., and Fanning, E. (2004). Cell cycle-dependent regulation of a human DNA helicase that localizes in DNA damage foci. Mol. Biol. Cell *15*, 3320–3332.

Hahn, A.T., Jones, J.T., and Meyer, T. (2009). Quantitative analysis of cell cycle phase durations and PC12 differentiation using fluorescent biosensors. Cell Cycle *8*, 1044–1052.

Hanahan, D., and Weinberg, R.A. (2011). Hallmarks of cancer: the next generation. Cell *144*, 646–674.

Hitomi, M., and Stacey, D.W. (1999). Cellular ras and cyclin D1 are required during different cell cycle periods in cycling NIH 3T3 cells. Mol. Cell. Biol. *19*, 4623–4632.

Hitomi, M., Yang, K., Guo, Y., Fretthold, J., Harwalkar, J., and Stacey, D.W. (2006). p27Kip1 and cyclin dependent kinase 2 regulate passage through the restriction point. Cell Cycle *5*, 2281–2289.

Johnson, D.G., Ohtani, K., and Nevins, J.R. (1994). Autoregulatory control of E2F1 expression in response to positive and negative regulators of cell cycle progression. Genes Dev. *8*, 1514–1525.

Justman, Q.A., Serber, Z., Ferrell, J.E., Jr., El-Samad, H., and Shokat, K.M. (2009). Tuning the activation threshold of a kinase network by nested feedback loops. Science *324*, 509–512.

Kinoshita, E., Yamada, A., Takeda, H., Kinoshita-Kikuta, E., and Koike, T. (2005). Novel immobilized zinc(II) affinity chromatography for phosphopeptides and phosphorylated proteins. J. Sep. Sci. *28*, 155–162.

Koff, A., Cross, F., Fisher, A., Schumacher, J., Leguellec, K., Philippe, M., and Roberts, J.M. (1991). Human cyclin E, a new cyclin that interacts with two members of the CDC2 gene family. Cell *66*, 1217–1228.

Lee, T.J., Yao, G., Bennett, D.C., Nevins, J.R., and You, L. (2010). Stochastic E2F activation and reconciliation of phenomenological cell-cycle models. PLoS Biol. *8*, e1000488.

Leung, J.Y., Ehmann, G.L., Giangrande, P.H., and Nevins, J.R. (2008). A role for Myc in facilitating transcription activation by E2F1. Oncogene *27*, 4172–4179.

Lin, R., Connolly, P.J., Huang, S., Wetter, S.K., Lu, Y., Murray, W.V., Emanuel, S.L., Gruninger, R.H., Fuentes-Pesquera, A.R., Rugg, C.A., et al. (2005). 1-Acyl-1H-[1,2,4]triazole-3,5-diamine analogues as novel and potent anticancer cyclin-dependent kinase inhibitors: synthesis and evaluation of biological activities. J. Med. Chem. *48*, 4208–4211.

Martinsson, H.S., Starborg, M., Erlandsson, F., and Zetterberg, A. (2005). Single cell analysis of G1 check points-the relationship between the restriction point and phosphorylation of pRb. Exp. Cell Res. *305*, 383–391.

McCusker, D., Denison, C., Anderson, S., Egelhofer, T.A., Yates, J.R., 3rd, Gygi, S.P., and Kellogg, D.R. (2007). Cdk1 coordinates cell-surface growth with the cell cycle. Nat. Cell Biol. *9*, 506–515.

Meijer, L., Borgne, A., Mulner, O., Chong, J.P., Blow, J.J., Inagaki, N., Inagaki, M., Delcros, J.G., and Moulinoux, J.P. (1997). Biochemical and cellular effects of roscovitine, a potent and selective inhibitor of the cyclin-dependent kinases cdc2, cdk2 and cdk5. Eur. J. Biochem. *243*, 527–536.

Merrick, K.A.A., Wohlbold, L., Zhang, C., Allen, J.J.J., Horiuchi, D., Huskey, N.E.E., Goga, A., Shokat, K.M.M., and Fisher, R.P.P. (2011). Switching Cdk2 on or off with small molecules to reveal requirements in human cell proliferation. Mol. Cell *42*, 624–636.

Morgan, D.O. (2007). The Cell Cycle: Principles of Control (New Science Press).

Naetar, N., Soundarapandian, V., Litovchick, L., Goguen, K.L.L., Sablina, A.A.A., Bowman-Colin, C., Sicinski, P., Hahn, W.C.C., DeCaprio, J.A.A., and Livingston, D.M.M. (2014). PP2A-mediated regulation of Ras signaling in G2 is essential for stable quiescence and normal G1 length. Mol. Cell *54*, 932–945.

Narasimha, A.M., Kaulich, M., Shapiro, G.S., Choi, Y.J., Sicinski, P., and Dowdy, S.F. (2014). Cyclin D activates the Rb tumor suppressor by monophosphorylation. eLife *3*, 3.

Pardee, A.B. (1974). A restriction point for control of normal animal cell proliferation. Proc. Natl. Acad. Sci. USA *71*, 1286–1290.

Pardee, A.B. (1989). G1 events and regulation of cell proliferation. Science *246*, 603–608.

Pardee, A.B., Dubrow, R., Hamlin, J.L., and Kletzien, R.F. (1978). Animal cell cycle. Annu. Rev. Biochem. *47*, 715–750.

Planas-Silva, M.D., and Weinberg, R.A. (1997). The restriction point and control of cell proliferation. Curr. Opin. Cell Biol. *9*, 768–772.

Polyak, K., Kato, J.Y., Solomon, M.J., Sherr, C.J., Massague, J., Roberts, J.M., and Koff, A. (1994). p27Kip1, a cyclin-Cdk inhibitor, links transforming growth factor-beta and contact inhibition to cell cycle arrest. Genes Dev. *8*, 9–22.

Quelle, D.E., Ashmun, R.A., Shurtleff, S.A., Kato, J.Y., Bar-Sagi, D., Roussel, M.F., and Sherr, C.J. (1993). Overexpression of mouse D-type cyclins accelerates G1 phase in rodent fibroblasts. Genes Dev. *7*, 1559–1571.

Raj, A., and van Oudenaarden, A. (2008). Nature, nurture, or chance: stochastic gene expression and its consequences. Cell *135*, 216–226.

Rao, R.N., Stamm, N.B., Otto, K., Kovacevic, S., Watkins, S.A., Rutherford, P., Lemke, S., Cocke, K., Beckmann, R.P., Houck, K., et al. (1999). Conditional transformation of rat embryo fibroblast cells by a cyclin D1-cdk4 fusion gene. Oncogene *18*, 6343–6356.

Rubin, S.M., Gall, A.L., Zheng, N., and Pavletich, N.P. (2005). Structure of the Rb C-terminal domain bound to E2F1-DP1: a mechanism for phosphorylation-induced E2F release. Cell *123*, 1093–1106.

Sage, J., Mulligan, G.J., Attardi, L.D., Miller, A., Chen, S., Williams, B., Theodorou, E., and Jacks, T. (2000). Targeted disruption of the three Rb-related genes leads to loss of G(1) control and immortalization. Genes Dev. *14*, 3037–3050.

Sakaue-Sawano, A., Kurokawa, H., Morimura, T., Hanyu, A., Hama, H., Osawa, H., Kashiwagi, S., Fukami, K., Miyata, T., Miyoshi, H., et al. (2008). Visualizing spatiotemporal dynamics of multicellular cell-cycle progression. Cell *132*, 487–498.

Sherr, C.J. (2000). The Pezcoller lecture: cancer cell cycles revisited. Cancer Res. *60*, 3689–3695.

Sherr, C.J., and Roberts, J.M. (1999). CDK inhibitors: positive and negative regulators of G1-phase progression. Genes Dev. *13*, 1501–1512.

Spencer, S.L.L., Cappell, S.D.D., Tsai, F.-C.C., Overton, K.W.W., Wang, C.L.L., and Meyer, T. (2013). The proliferation-quiescence decision is controlled by a bifurcation in CDK2 activity at mitotic exit. Cell *155*, 369–383.

Stein, G.H. (1979). T98G: an anchorage-independent human tumor cell line that exhibits stationary phase G1 arrest in vitro. J. Cell. Physiol. *99*, 43–54.

Vassilev, L.T., Tovar, C., Chen, S., Knezevic, D., Zhao, X., Sun, H., Heimbrook, D.C., and Chen, L. (2006). Selective small-molecule inhibitor reveals critical mitotic functions of human CDK1. Proc. Natl. Acad. Sci. USA *103*, 10660–10665.

Welcker, M., and Clurman, B. (2005). Cell cycle: how cyclin E got its groove back. Curr. Biol. *15*, R810–R812.

Yang, H.W., Chung, M., Kudo, T., and Meyer, T. (2017). Competing memories of mitogen and p53 signalling control cell-cycle entry. Nature *549*, 404–408.

Yao, G., Lee, T.J., Mori, S., Nevins, J.R., and You, L. (2008). A bistable Rb-E2F switch underlies the restriction point. Nat. Cell Biol. *10*, 476–482.

Yen, A., and Pardee, A.B. (1978). Exponential 3T3 cells escape in mid-G1 from their high serum requirement. Exp. Cell Res. *116*, 103–113.

Zetterberg, A., and Larsson, O. (1985). Kinetic analysis of regulatory events in G1 leading to proliferation or quiescence of Swiss 3T3 cells. Proc. Natl. Acad. Sci. USA *82*, 5365–5369.

Zetterberg, A., and Larsson, O. (1991). Coordination between cell growth and cell cycle transit in animal cells. Cold Spring Harb. Symp. Quant. Biol. *56*, 137–147.

Zetterberg, A., Larsson, O., and Wiman, K.G. (1995). What is the restriction point? Curr. Opin. Cell Biol. *7*, 835–842.

Zwang, Y., Sas-Chen, A., Drier, Y., Shay, T., Avraham, R., Lauriola, M., Shema, E., Lidor-Nili, E., Jacob-Hirsch, J., Amariglio, N., et al. (2011). Two phases of mitogenic signaling unveil roles for p53 and EGR1 in elimination of inconsistent growth signals. Mol. Cell *42*, 524–535.

STAR★METHODS

KEY RESOURCES TABLE

REAGENT or RESOURCE	SOURCE	IDENTIFIER
Antibodies		
Rabbit polyclonal anti-mCherry	Abcam	Cat#ab167453; RRID: AB_2571870
Goat anti-rabbit IRDye 800CW	LI-COR Biosciences	Cat#926-32211; RRID: AB_621843
Chemicals, Peptides, and Recombinant Proteins		
3xFLAG-cyclin D1-Cdk4	This paper	N/A
3xFLAG-cyclin E1-Cdk2	This paper	N/A
3xFLAG-cyclin E1-Cdk1	This paper	N/A
3xFLAG-cyclin A2-Cdk2	This paper	N/A
3xFLAG-cyclin A2-Cdk1	This paper	N/A
3xFLAG-cyclin B1-Cdk2	This paper	N/A
3xFLAG-cyclin B1-Cdk1	This paper	N/A
6xHis-HDHB-EGFP (aa 994-1087 of human DHB)	This paper	N/A
6xHis-RbC (aa 771-928 of human Rb)	This paper	N/A
Histone H1	EMD Millipore	Cat#14-155
Lambda Protein Phosphatase	New England BioLabs	Cat#P0753S
Experimental Models: Cell Lines		
WI-38	Harbury Lab (Stanford)	RRID: CVCL_0579
MRC5-hTert	Santos Lab (UMDNJ)	N/A
RPE1-hTERT	Stearns Lab (Stanford)	RRID: CVCL_4388
T98G	ATCC	Cat#CRL-1690; RRID: CVCL_0556
Cdk2^{as} RPE cells	Fisher Lab (Mt. Sinai) (Merrick et al., 2011)	N/A
Primary human foreskin fibroblasts	Khavari Lab (Stanford)	N/A
Primary human fetal lung fibroblasts	Cell Applications	Cat#506-05f
Recombinant DNA		
CSII-EF1alpha-MCS	Riken	Cat#RDB04378
CSII-EF1alpha-HDHB-EGFP	This paper	N/A
CSII-EF1alpha-HDHB-mCherry	This paper	N/A
CSII-EF1alpha-Geminin-GFP	This paper	N/A
CSII-E2F1pr-EGFP-PEST-NLS	This paper	N/A
pGAL1-3Flag-CycD1-L-Cdk4-pRS425	This paper	N/A
pGAL1-3Flag-CycE1-L-Cdk2-pRS425	This paper	N/A
pGAL1-3Flag-CycE1-L-Cdk1-pRS425	This paper	N/A
pGAL1-3Flag-CycA2-L-Cdk2-pRS425	This paper	N/A
pGAL1-3Flag-CycA2-L-Cdk1-pRS425	This paper	N/A
pGAL1-3Flag-CycB1-L-Cdk2-pRS425	This paper	N/A
pGAL1-3Flag-CycB1-L-Cdk1-pRS425	This paper	N/A
pMK183 HDHB-EGFP-pET28a	This paper	N/A
pMK182 RbC-pET28a	This paper	N/A
Software and Algorithms		
MATLAB	MathWorks	www.mathworks.com/products/matlab.html
Bistable Rb-E2F switch ordinary differential equation model	Yao et al., 2008	www.ebi.ac.uk/biomodels-main/BIOMD0000000318

CONTACT FOR REAGENT AND RESOURCE SHARING

Further information and requests for resources and reagents should be directed to and will be fulfilled by the Lead Contact, Jan M. Skotheim (skotheim@stanford.edu).

EXPERIMENTAL MODEL AND SUBJECT DETAILS

Cell line and primary cell culture

WI-38 cells were obtained from the Harbury Lab (Stanford), MRC5-hTert cells from the Santos Lab (UMDNJ), RPE1-hTert lines from the Stearns Lab (Stanford) and the Cleveland Lab (UCSD), Cdk2^{as} RPE-hTERT cells from the Fisher Lab (Mount Sinai), and T98G cells from ATCC. Recently isolated primary human foreskin fibroblasts (HFF) were obtained from the Khavari Lab (Stanford), and recently isolated fetal human lung fibroblasts (HLF), were obtained from Cell Applications. RPE1-hTert cells were cultured in DMEM/F12 (Corning) with 10% FBS (Cellgro) and 1% Penicillin/Streptomycin (Cellgro). WI-38 cells were cultured in MEM (GIBCO), 10% FBS, 1% Penicillin/Streptomycin, 1% non-essential amino acids, and 1% sodium pyruvate. MRC5-hTert, T98G, Cdk2^{as} RPEs, and HFFs were cultured in DMEM (Cellgro), 10% FBS, and 1% Penicillin/Streptomycin. Primary lung fibroblasts were cultured in Cell Applications' lung fibroblast medium for the first passage, and subsequent passages and experiments were performed in DMEM, 10% FBS, and 1% Penicillin/Streptomycin. Only primary cells under passage seven were used for experiments. WI-38, RPE-hTERT, and HLF were female. MRC5-hTERT, T98G, and HFF were male.

METHOD DETAILS

Fluorescent reporters

Fluorescent reporters (HDHB-EGFP, HDHB-mCherry, E2F1pr-EGFP-PEST, cyclin E pr-cyclin E-EGFP-PEST, and geminin-GFP) were cloned into the CSII-EF-MCS lentiviral vector backbone. The CSII vector, the packaging vector dr8.74 and the envelope vector VSVg were introduced into 293T HEK cells by transfection with TurboFect (Life Technologies). For each microscopy experiment, medium from transfected 293T cells was used to infect passage 3 HLFs (transduction efficiency was ~20%). We began imaging 2 days following infection.

To measure E2F1 promoter activation, we used a 796 base pair fragment upstream of the E2F1 transcription start site driving expression of an EGFP protein that was destabilized by fusion to the 120 base pairs encoding amino acids 422-461 of mouse ornithine decarboxylase which includes a PEST degradation domain from amino acids 423-449 (EGFP-MODC-(422-461) from (Corish and Tyler-Smith, 1999), here called EGFP-PEST). This fragment was designed to contain all the regulatory elements in the E2F1 promoter identified in a previous study (Johnson et al., 1994). In addition, the construct was fused to an N-terminal nuclear localization signal (NLS) to facilitate fluorescence quantification. A similar live-cell reporter of E2F1 transcription based on a 784 base pair fragment of the E2F1 promoter was recently examined by another group (Dong et al., 2014).

Microscopy

In preparation for imaging, cells were seeded at a density of approximately 100,000 per 35-mm collagen-coated glass-bottom dish (MatTek) and incubated overnight in a 37°C, 5% CO2 incubator. Images were taken for up to 9 positions per dish, for 3 dishes, every 30 minutes with a Zeiss AxioVert 200M microscope with an automated stage using an EC Plan-Neofluar 5x/0.16NA Ph1 objective or an A-plan 10x/0.25NA Ph1 objective. HLFs expressing GFP-fusion fluorescent reporters were exposed for 1 s using the Colibri LED 470 module at 100% power.

Image analysis

HDHB-EGFP images were manually segmented in ImageJ using phase and fluorescence images to identify nucleus and cytoplasm. The median nuclear and cytoplasmic signal intensities for individual cells over the course of an experiment were measured, the local median background intensity was subtracted, and the ratio of cytoplasmic-to-nuclear GFP signal was used as a surrogate for Cdk activity as in another study (Spencer et al., 2013). For cells expressing Geminin-GFP, nuclei were segmented and tracked using a semi-automated custom MATLAB algorithm adapted from our previous work (Doncic et al., 2013). Cells expressing E2F1pr-EGFP-PEST were tracked and segmented manually.

Transcriptional activation analysis

To determine the timing of E2F1pr-EGFP-PEST activation, we employed an automated algorithm described in our previous work (Eser et al., 2011). This algorithm fits a smoothing spline (implemented in MATLAB with smoothing parameter 0.7) to the data. Next, the maximum of the second derivative of the spline fit was taken as the activation time.

Cdk activity threshold analysis

In serum removal and MEK inhibitor addition experiments, cells were tracked from their last division prior to the condition change until their next division or the end of the experiment (24-48 hours after medium change). Cdk activity was measured as described above

and cells were classified by whether or not they divided after the medium change. The Cdk activity traces were smoothed using a 3-time point sliding window. A logistic regression was used to estimate the probability that a cell would divide again after the medium change as a function of the Cdk activity at the time of the medium change. We defined the Cdk activity threshold as the point where our logistic regression estimated 50% of the cells were committed to division. The accuracy of each threshold was determined by assigning cell fates based on whether each cell is above or below the threshold at the time of medium exchange, and then calculating what percent of cell fates (divide once more or immediately arrest) were correctly assigned. We performed a cross validation analysis as follows. First, we determined a threshold as described above using the dataset excluding a single data point. Next, we used this threshold to predict the fate of the excluded cell. This yielded a ~4% error rate for the serum removal data consistent with the analysis of the full dataset performed as described above. Error bars on the logistic regression were calculated by bootstrapping. We generated 1000 datasets by sampling of our data with replacement. We then performed a logistic regression on each bootstrap sample. In Figures 3I, 5D, and S3I, we plotted the median and 95% confidence intervals for this set of logistic regressions.

Protein expression and purification

For *in vitro* kinase assays, N-terminally His6-tagged recombinant HDHB-EGFP (aa 994-1087 from HDHB) and RbC (aa 771-928 of Rb) (Adams et al., 1999; Rubin et al., 2005) were purified by cobalt-Sepharose affinity chromatography (GE Sepharose cat#17-0575-01) and eluted with 200 mM imidazole. Histone H1 protein (EMD Millipore) was used as a general substrate for Cdk. Human cyclin-Cdk fusion complexes were purified from yeast cells using a FLAG-tag method, modified from a previous protocol used for HA-tag purification (McCusker et al., 2007). Briefly, N-terminally tagged cyclin-Cdk fusions were cloned into 2-micron vectors using a glycine-serine linker (Rao et al., 1999) and overexpressed from the *GAL1* promoter. The overexpressed 3xFLAG-tagged cyclin-Cdk complexes were then purified by immunoaffinity chromatography using anti-FLAG-M2 affinity agarose beads (Sigma-Aldrich A2220) and eluted with 0.2 mg/mL 3xFLAG peptide (Sigma-Aldrich F4799). We note that similar Cdk/cyclin fusions have been able to restore wild-type function *in vivo* (Chytil et al., 2004).

In vitro kinase assay

For the *in vitro* phosphorylation assays with HDHB-EGFP and RbC proteins, substrate concentrations were kept in the range of 1-5 μM. Approximately equal amounts of purified kinase complexes were used, with the exception of Cdk4/cyclin D1, which was about 10-fold in excess compared to other complexes. Reaction aliquots were taken at two time points (8 and 16 min) and the reaction was stopped with SDS-PAGE sample buffer. The basal composition of the assay mixture contained 50 mM HEPES, pH7.4, 180 mM NaCl, 5 mM $MgCl_2$, 20 mM imidazole. 0.2 mg/ml FLAG peptide, 2% glycerol, 3 mM EGTA, 0.2 mg/ml BSA and 500 uM ATP (with 2 μCi of [γ-32P] ATP added per reaction (PerkinElmer cat# BLU502Z250UC)). To separate the phosphorylated proteins, 10% SDS-PAGE was used for HDHB-EGFP and H1 and 15% SDS-PAGE was used for RbC. Phosphorylation of substrate proteins was visualized using autoradiography (Typhoon instrument; GE Healthcare).

Phos-tag SDS-PAGE and phosphatase assay

HLFs were collected and lysed in lysis buffer containing urea for Figure 6E or in RIPA buffer for the phosphatase assay in Figure S6F. For the phosphatase assay, 40 μL of RIPA buffer lysates were incubated overnight at 30°C with 5 μL of Lambda Protein Phosphatase (400,000 units/mL; New England Biolabs). Phosphorylated species of HDHB-mCherry were resolved from the lysates with Phos-tag SDS-PAGE (Kinoshita et al., 2005) and quantified using ImageJ. The concentration of the Phos-tag in 10% SDS-PAGE was 50 μM. Blotting of Phos-tag SDS-PAGE gels was performed with a dry system iBlot2 (Invitrogen by Thermo Fisher Scientific). Abcam anti-mCherry polyclonal antibody (1:1000) (cat. no. ab167453) and IRDye 800CW goat anti-rabbit antibody (1:20000) from LI-COR Biosciences (cat. no. 926-32211) were used for the detection of mCherry-tagged HDHB.

Prediction framework

The high temporal resolution of molecular events in single-cell assays allows a very precise inference of which of these molecular events determine cell fate (Doncic and Skotheim, 2013; Doncic et al., 2011, 2015). Such inferences cannot be made with techniques where population heterogeneity blurs the dynamics of cellular transitions. Our assay includes two essential components: (1) Expose cells to an abrupt step change in their extracellular environment and observe subsequent cell fate (divide or not); (2) Use only information prior to the step change to predict subsequent cell fate. Regarding (1), without a step change decreasing growth factor signaling the location of commitment in the cell cycle cannot be measured. Fixation of cells expressing fluorescent reporters can be used to correlate dynamic aspects of cell signaling activities with other cell-cycle events, such as DNA replication. For example, this was recently used to show that the onset of DNA replication correlates with low levels of E2F1 expression (Dong et al., 2014). However, since the serum removal experiment was not performed, we do not know where commitment takes place in this set of experiments. Regarding point (2), tracking cell fate and using subsequent information can result in conflating downstream molecular events with an upstream decision. For example, it was recently shown that Cdk activity correlated with rapid cell-cycle progression in immortal cells (Spencer et al., 2013). However, these cells are already committed to division ~4 hours before the mitosis of the preceding cell cycle and are already on a trajectory to divide prior to the Cdk activity measurement just after mitosis. Thus, the Cdk activity 4 hours after commitment to division, which was used for predictive purposes, is more likely a consequence of some preceding molecular event that occurred in the previous cell cycle that committed the cell to division.

FACS analysis

Cells were prepared for FACS analysis by washing with 1X PBS, trypsinizing, and resuspending in 1X PBS. Vybrant DyeCycle orange dye (Invitrogen) was diluted 1:1000 into the cell suspension and incubated for 30 minutes at 37°C. After incubation, cells were washed twice with 1X PBS, resuspended in 0.5 mL 1X PBS, and transferred to FACS tubes (BD Falcon). FACS analysis was performed on a FACSCalibur machine (BD Biosciences), and data were analyzed using the FlowJo cell-cycle analysis feature (Tree Star).

ODE model of R

We used the previously published model by Yao et al. (2008). To accommodate our experimental results we modified the model in two ways indicated by orange arrows in Figure 7A:

(i) To reconcile the experimental observation that post-R cells continue through the cell cycle despite complete serum removal, we added a serum-independent *E2F* transcription rate, k_{pfb}. Note that in the original model, all *E2F* transcription depends on serum so that the model is not bistable at 0% serum (Figure S7A).

(ii) To account for the lower commitment threshold when cells are exposed to a MEK inhibitor, we separated the growth signals into a MEK-dependent and a MEK-independent part. This results in a lower Cdk activity threshold for commitment in response to MEK inhibition than serum removal, as we observed.

Given our interpretation of the Cdk activity sensor's specificity, we also interpret the CE term as a composite of Cdk2 and Cdk1 activities with cyclins E and A.

Differential Equations Model
$\frac{d[M]}{dt} = \frac{k_M[M]}{K_S + [S]} - d_M[M]$
$\frac{d[E]}{dt} = k_E\left(k_{pfb} + \frac{[M]}{K_M + [M]}\right)\left(\frac{[E]}{K_E + [E]}\right) + \frac{k_b[M]}{K_M + [M]} + \frac{k_{p1}[CD][RE]}{K_{CD} + [RE]} + \frac{k_{p2}[CE][RE]}{K_{CE} + [RE]} - d_E[E] \quad - k_{RE}[R][E]$
$\frac{d[CD]}{dt} = \frac{k_{CD}[M]}{K_M + [M]} + \frac{k_{CDS}[S]}{K_S + [S]} - d_{CD}[CD]$
$\frac{d[CE]}{dt} = \frac{k_{CE}[E]}{K_E + [E]} - d_{CE}[CE]$
$\frac{d[R]}{dt} = k_R + \frac{k_{DP}[RP]}{K_{RP} + [RP]} - k_{RE}[R][E] - \frac{k_{p1}[CD][R]}{K_{CD} + [R]} - \frac{k_{p2}[CE][R]}{K_{CE} + [R]} - d_R[R]$
$\frac{d[RP]}{dt} = \frac{k_{p1}[CD][R]}{K_{CD} + [R]} + \frac{k_{p2}[CE][R]}{K_{CE} + [RE]} + \frac{k_{p1}[CD][RE]}{K_{CD} + [RE]} + \frac{k_{p2}[CE][RE]}{K_{CE} + [RE]} - d_{RP}[RP]$
$\frac{d[RE]}{dt} = k_{RE} - \frac{k_{p1}[CD][RE]}{K_{CD} + [RE]} + \frac{k_{p2}[CE][RE]}{K_{CE} + [RE]} - d_{RE}[RE]$

We use the same notation as Yao et al. (2008): S = growth signals (e.g., serum), M = Myc, E = E2F, CD = CycD, CE = CycE, R = unphosphorylated (active) Rb, RP = phosphorylated (inactive) Rb, RE = Rb-E2F complex. The initial conditions used were: [Rb] = 0.55 μM and all other concentrations were set to zero. Serum concentration was taken to be 2% unless otherwise stated. Except the k_{pfb} term, the equations are the same the original model (Yao et al., 2008).

Rate	Value
k_E	0.4 μM/hr
k_M	1.0 μM/hr
k_{CD}	0.03 μM/hr
k_{CDS}	0.45 μM/hr
k_R	0.18 μM/hr
k_{RE}	180 μM/hr
k_b	0.003 μM/hr
K_S	0.5 μM
k_{CE}	0.35 μM/hr

(*Continued on next page*)

Continued	
Rate	Value
d_M	0.7/hr
d_E	0.25/hr
$d_{CD} = d_{CE}$	1.5/hr
$d_R = d_{RP}$	0.06/hr
d_{RE}	0.03/hr
$k_{P1} = k_{P2}$	18/hr
k_{DP}	3.6 μM/hr
$K_M = K_E$	0.15 μM
$K_{CD} = K_{CE}$	0.92 μM
K_{RP}	0.01 μM
k_{pfb}	4 μM

All rates except k_{pfb}, which we added to the model, were the same as in the original model (Yao et al., 2008). This system of ODEs was solved using the Runge-Kutta algorithm implemented using MATLAB.

Computation of commitment thresholds: The model was solved with the specified initial conditions and 2% serum for variable durations after which serum is decreased to 0% (see schematic in Figure 7B). In cases where the simulation passed the point of commitment before serum was removed, *CE* eventually reached a high steady-state value. If the threshold was not passed, *CE* returned to its initial value of zero (e.g., red and blue curves in Figure 7B). For consistency, we used the same 'high' serum concentration (2%) as in Yao et al. (2008). To simulate the effect of the MEK inhibitor we lowered the serum concentration to 0.28% instead of 0% to fit our experimental results.

Comparison of ODE model results with our experiments: To scale the *CE* term from the model into the experimentally measured units of Cdk activity, we first calculated the mean peak Cdk activity for cells that passed R and the baseline Cdk activity for cells that failed to pass R (from the cells in Figure 3G). These activities were 1.83 ± 0.06 (mean ± standard error of the mean, n = 44) and 0.51 ± 0.01 (mean ± standard error of the mean, n = 58) respectively. The range of *CE* was scaled to be between these values so that model and experimental results can be compared (Figure 7C).

QUANTIFICATION AND STATISTICAL ANALYSIS

Statistical details of experiments (p values, confidence intervals from bootstrap analyses, sample sizes) can be found in the figure legends. Statistical tests (Chi-square tests in Figures 2E and 2H, KS tests in Figure S3B, t test in Figure 4D) were performed in MATLAB. 95% confidence intervals were calculated through bootstrap analyses for the logistic regressions and corresponding threshold determinations in Figures 3I and 5D. 50% confidence intervals were calculated for the probabilities estimated in Figure 6C. All bootstrapped confidence intervals were determined by sampling with replacement 1000 times from the relevant datasets (cellular Cdk activities at the time of serum removal or MEK inhibitor addition for Figures 3I and 5D; binary data describing whether each cell divided after treatment with 3-MB-PP1 or DMSO for Figure 6C).